






Model Validation for Quantitative X-Ray Measurements

L. M. Reusch, P. Franz, D. J. Den Hartog, J. A. Goetz, M. D. Nornberg & P. VanMeter


To cite this article: L. M. Reusch, P. Franz, D. J. Den Hartog, J. A. Goetz, M. D. Nornberg & P. VanMeter (2018) Model Validation for Quantitative X-Ray Measurements, Fusion Science and Technology, 74:1-2, 167-176, DOI: [10.1080/15361055.2017.1404340](https://doi.org/10.1080/15361055.2017.1404340)

To link to this article: <https://doi.org/10.1080/15361055.2017.1404340>

 View supplementary material 

 Published online: 21 Feb 2018.

 Submit your article to this journal 

 Article views: 39

 View Crossmark data 



Model Validation for Quantitative X-Ray Measurements

L. M. Reusch,^{a*} P. Franz,^b D. J. Den Hartog,^a J. A. Goetz,^a M. D. Nornberg,^a and P. VanMeter^a

^aUniversity of Wisconsin–Madison, Department of Physics, Madison, Wisconsin 53706

^bConsorzio RFX, EURATOM-ENEA Association, Padova, Italy

Received July 19, 2017

Accepted for Publication October 26, 2017

Abstract — *Soft-X-ray (SXR) brightness measurements contain information on a number of physics parameters in fusion plasmas; however, it is nearly impossible to extract the information without modeling. A validated forward model is therefore necessary for the accurate interpretation of SXR measurements and will be critical in the burning plasma era, where medium- and high-Z impurities are ever present. The Atomic Data and Analysis Structure (ADAS) database is a powerful interpretive tool that is extensively used to model and predict atomic spectra, level populations, and ionization balance for fusion plasmas. These predictions are in good agreement with experimental measurements. However, continuum radiation in the X-ray range, while also modeled in ADAS, has not been rigorously verified or tested against experimental data. We therefore performed a systematic comparison of ADAS to a simplified model called PFM. PFM only calculates continuum radiation but shows good agreement with experimental data when only continuum radiation is present. ADAS and the simplified model agree to within 1% to 2% indicating that ADAS is calculating continuum radiation correctly. We have also begun a validation of SXR brightness calculations from ADAS. The SXR brightness measurements modeled by ADAS agree well with experimental measurements from an extreme where the signal is dominated by line radiation continuously through another extreme where the signal is dominated by continuum emission. While this validation work is preliminary, it strongly suggests that ADAS accurately models the physics that lead to SXR radiation.*

Keywords — *X-ray brightness, collisional-radiative modeling, validation.*

Note — *Some figures may be in color only in the electronic version.*

I. INTRODUCTION

Soft-X-ray (SXR) brightness measurements are sensitive to many plasma parameters of interest, but to take advantage of the wealth of information embedded in those measurements, absolute SXR brightness measurements must be combined with information from modeling. SXR radiation is dependent on electron temperature T_e , electron density n_e , neutral density n_D , and impurity content n_z and thus the effective ionic charge of the plasma. SXR measurements provide qualitative information about the internal structure of the magnetic field assuming that n_e , T_e , and n_z are all constant on a magnetic flux surface.^{1–5} Additionally, electron temperature can be inferred via the two-color technique,^{6,7} but this assumes the SXR spectrum contains only continuum

radiation (e.g., bremsstrahlung). In machines with only low-Z plasma-facing components, these assumptions are typically met; however, many candidate materials for future machines are much higher-Z, and therefore, the plasmas will likely contain some high-Z impurities. In these cases, it is likely that n_z will not be constant on a flux surface, as has been previously seen.^{8–10} Additionally, high-Z materials emit atomic line radiation and other noncontinuum radiation up to very high photon energies, so the X-ray spectrum will not contain only continuum radiation.

Absolute measurements of SXR radiation remove the need to assume that the SXR spectrum contains only continuum radiation and provides constraints on n_e , n_z , and n_D profiles in addition to T_e . These absolute measurements require additional calibrations compared with relative measurements; however, such calibrations for SXR brightness can be straightforward. This additional calibration effort is worthwhile as X-rays are intrinsically generated,

*E-mail: lm McGuire@wisc.edu

allowing access to information about these plasma parameters without the need for concurrent operation of lasers or neutral beams.

While absolute measurements of SXR radiation can be straightforward, interpretation of such measurements is nearly impossible without using information from modeling. Many different sources of radiation that depend on different atomic processes contribute to the SXR signal. Free-free bremsstrahlung, radiative and dielectronic recombination, and atomic line radiation can all contribute, depending on the impurities present. Free-free and radiative recombination radiation are straightforward to calculate, but dielectronic and line radiation depend sensitively on the surrounding plasma environment.^{11–15} Furthermore, n_D affects everything as charge exchange with neutral particles affects the charge state balance of higher- Z impurity species.

The example SXR spectrum shown in Fig. 1 illustrates the inherent complexity when medium- or high- Z impurities are present. This spectrum was created using plasma parameters from the high-confinement regime of the Madison Symmetric Torus^{16,17} (MST), which is a medium-sized reversed-field pinch that has a closely fitting aluminum (Al) shell that acts as the plasma first wall. Aluminum is always present in MST plasmas, with different levels of concentrations depending on the plasma conditions. Aluminum emission lines and recombination

steps are clearly visible around 2 keV. The free-free background is shown as the dashed line (red), which is much smaller than the total radiation (solid, blue). Several low- Z impurities (B, N, C, and O, which arise from other plasma-facing components or are atmospheric contaminants) also contribute to the spectrum and must be taken into account in order to accurately match absolute measured brightness. Low-energy photons such as visible and extreme ultraviolet (XUV) photons (gray box) are outside the range of interest and are typically filtered out. MST is an excellent machine on which to validate a quantitative SXR brightness model because all impurities in MST have been well studied.^{18–20} Furthermore, the presence of a single medium- Z impurity Al can act as a proxy for higher- Z materials. For the plasma conditions used in this example and throughout the rest of this paper, in the core of the plasma, all low- Z impurities have been fully ionized, and roughly 30% of the Al has been fully ionized.

Because of the complex interdependence of the atomic physics and plasma environment, a suitable model to use as an aid in interpreting SXR brightness measurements must be a collisional-radiative model that takes into account the charge exchange with neutral particles. The Atomic Data and Analysis Structure database²¹ (ADAS) is one such model. There are many other models, but they will not be discussed here. ADAS calculates excited level populations,

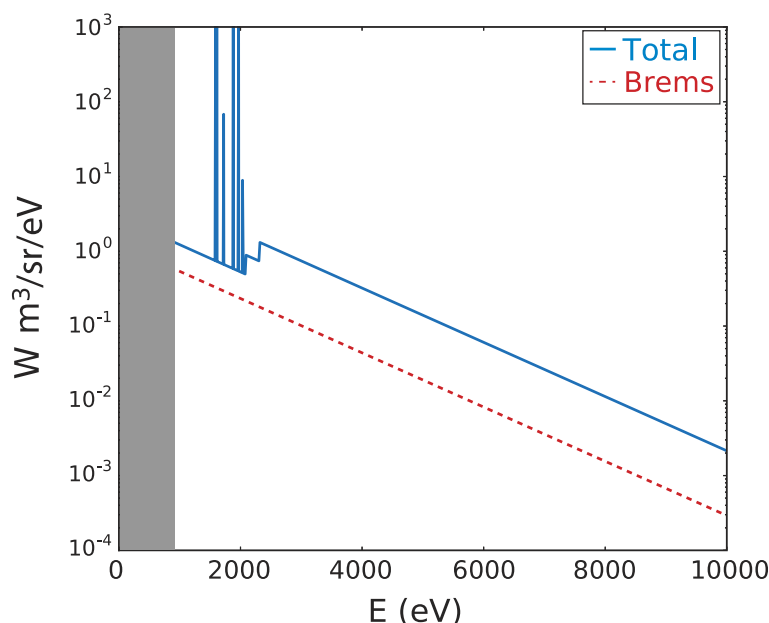


Fig. 1. An example SXR spectrum containing B, N, C, O, and Al impurities. Solid curve (blue line) is total emissivity that is measured, compared to the free-free bremsstrahlung (dashed, red line) that is often assumed to be the main source of radiation in this energy range. Discrete radiation lines and recombination steps from Al are present. The absolute amplitude is also affected by the presence of the low- Z impurities in the plasma, but there are no recombination steps or emission lines in this energy range for those impurities.

ionization balance, dielectronic recombination, line spectra, and total line radiation that might come from a wide range of plasma environments, from astrophysics to laboratory plasmas, with major application in fusion. Those quantities have also all been compared fairly extensively to data and agree well.^{12,15,22–26} ADAS also calculates free-free and radiative recombination,²⁷ but these calculations have not been extensively compared to data. In order to use ADAS as an aid in interpreting SXR measurements, all parts of ADAS need to be verified and validated. This work therefore presents a verification of the free-free and radiative recombination radiation calculations and a comparison of ADAS modeling to SXR brightness measurements.

II. VERIFICATION OF ADAS

A first step to use ADAS as an interpretive model is to verify that free-free and radiative recombination emission are being calculated correctly. As both radiative recombination and free-free radiation involve free electrons from the continuum, they will collectively be referred to here as continuum radiation. As noted above, continuum radiation can be straightforward to calculate; however, it is important to make sure it is being done correctly, and to our knowledge, this has not been done. We also note that verification of noncontinuum sources of radiation and other collision-dependent quantities from ADAS is outside the scope of this verification and are generally assumed to be suitably accurate due to the long history of comparison to data for those quantities. For the verification of continuum radiation, we compared results from ADAS to an in-house model that has long been used to interpret SXR data where we expect only continuum radiation to be present. This model was originally written by P. Franz of Consorzio RFX and is referred to here as PFM for conciseness.

PFM (Refs. 28 and 29) calculates free-free and radiative recombination emission assuming a Maxwellian electron distribution. For a given ion of charge x , this is³⁰

$$\epsilon_x = \frac{1}{4} K \frac{n_e n_x Z^2}{T_e} e^{-E/T_e} \left[g_{ff} + g_{fb} \frac{\xi}{n^3} \frac{\chi}{T_e} e^{\chi/T_e} \right] \frac{2Z^2 R_y}{v^3 T_e} e^{Z^2 R_y / v^2 T_e} dE ;$$

where

$$K = \text{physical constant} = 1.52 \times 10^{38} \text{ W m}^3 / \text{sr eV}$$

- n_e = electron density
- n_x = density of the ion in question
- Z = ionic charge
- n = principal quantum number of the lowest unfilled shell
- ξ = number of holes in the lowest unfilled shell
- χ = recombination energy
- R_y = Rydberg constant
- g_{ff}, g_{fb} = free-free and free-bound Gaunt factors, respectively,

and the integral is over all photon energies E .

A complete description of how recombination radiation was implemented in PFM can be found in Ref. 29.

A description of how continuum radiation has been implemented in ADAS can be found in Ref. 27. The main difference between the two models is in the treatment of recombination radiation and the limits of the spectral integration. In PFM only the first five quantum states are included in the sum, but ADAS has a temperature-dependent criterion for truncating the sum. Regarding the integration over photon energies, PFM was designed to be used with a modeled instrument function, making numerical integration possible between a lower bound of 10 eV and an upper bound of 10 keV. These limits were chosen such that at the low-energy cutoff, the filter transmission is negligible, and at the high-energy cutoff, the detector absorption is negligible. An instrument response can be included in ADAS, but it is also possible to calculate the spectral integral without any filter or detector. This is accomplished through application of the first exponential integral.

While a full discussion of Gaunt factors is outside the scope of this paper, it should be noted that PFM can use either a Born approximation for g_{ff} or values interpolated from Van Hoof et al.³¹ The free-bound Gaunt factor is equal to 1. ADAS uses free-free Gaunt factors from Karzas and Latter,³² which agree well with those in Van Hoof et al. All comparisons here are made with PFM using Gaunt factors from Van Hoof et al.

The emissivity for a given atomic element z is the sum of Eq. (1) over each charge state x of element z :

$$\epsilon_z = \sum_x \frac{1}{4} n_e n_x P_x ;$$

However, n_x depends on the total density for element z and the fractional abundance of charge state x . To highlight this, Eq. (2) can be written as

$$\epsilon_z \approx \frac{1}{4} n_e n_z \sum_x \frac{n_x}{n_z} P_x ; \quad (3)$$

where

n_z = total density for the element

n_x/n_z = fraction of ions in charge state x (i.e., the fractional abundance)

P_x = coefficient that includes the rest of the terms in Eq. (1).

The sum over charge states can be combined into a coefficient quantifying the radiated power for an element as a whole. This recombination and bremsstrahlung power coefficient (PRB) is thus defined as

$$\text{PRB} \approx \frac{1}{4} \sum_x \frac{n_x}{n_z} P_x ; \quad (4)$$

PFM does not calculate ionization balance; rather, all density profiles are specified by the user. For the impurities found in MST, PFM assumes fully ionized low- Z impurities (B, C, N, and O) based on previous impurity studies in similar plasma conditions.^{18,20} Aluminum densities are specified with an ionization balance also based on experimental measurements in similar conditions that show that an ionization balance for Al is consistent with ADAS predictions.¹⁹ The predicted emissivity based on the user-defined profiles is then integrated along the line of sight for each detector, treating each line of sight as a pencil beam. A more complete discussion of how the plasma parameter profiles and possible poloidal asymmetries are incorporated into the model can be found in Ref. 28.

This model has long been used to infer T_e from SXR measurements using the two-color technique. The inferred electron temperatures typically agree very well with Thomson scattering measurements, indicating that PFM accurately models the continuum for multiple energy ranges. The absolute brightness also matches experimental data. Figure 2 shows an example of the agreement between PFM (red triangles) and SXR data (black circles) for two cases where no noncontinuum radiation was present. Figure 2a shows results from RFX-mod, which has a carbon first wall and thus has no medium- or high- Z impurities. Agreement can also be attained in MST as illustrated in Fig. 2b despite the Al first wall, by filtering out noncontinuum sources of radiation. Here, noncontinuum sources of radiation were filtered out using thick beryllium (Be) filters of 400 and 800 μm (10% cutoff energies of 2700 and 3300 eV, respectively). This agreement between PFM and experimental SXR measurements for multiple machines gives us

confidence that PFM is a good model with which to verify the calculation of free-free and radiative recombination in ADAS.

The comparison between PFM and ADAS used the PRB values as defined in Eq. (4). This was done for each impurity (B, C, N, O, and Al) as well as the majority ion: deuterium. The comparison was performed over a range in T_e of 10 to 3200 eV. Given the requirement that PFM include an instrument response, we used three different Be filter thicknesses in both PFM and ADAS: 5, 85, and 800 μm with a 35- μm Si detector. The results in Fig. 3 show example results using an 85- μm filter; however, similar levels of agreement were found for all ions and filter thicknesses.

A temperature range was chosen to check that ADAS and PFM agree where PFM is known to be valid ($T_e \geq 500$ eV) and disagree for lower temperatures. We compared free-free and radiative recombination components separately, as well as the total. For all elements, ADAS and PFM agree with each other within 1% to 2% for $T_e \geq 500$ eV. Figure 3 shows an example of this agreement for carbon. The top row shows the PRB as a function of T_e for ADAS (solid, black), PFM (dashed, red), and the absolute difference (dash-dot, green). The curves for ADAS and PFM are nearly indistinguishable because of the strong agreement. The bottom row shows the percent difference between ADAS and PFM. The columns correspond to the total radiated power, free-free, and radiative recombination for left, center, and right columns, respectively.

III. COMPARISON TO EXPERIMENT

The preliminary validation of SXR brightness models from ADAS used experimental measurements from the two-color SXR tomography system on MST (Refs. 33 and 34). The SXR tomography system has four cameras with a pair of ten absolute XUV diode arrays arranged such that there are 40 unique lines of sight, and each line of sight has two diodes (a total of 80 measurements). For two-color operation, we typically aim to filter out the Al line emission by equipping one diode array on each camera with a 400- μm Be filter and the other with an 800- μm Be filter.

For this work, however, we installed a different-thickness Be filter on each diode array. This gives eight different cutoff energies effectively forming a very coarse spectrometer. Despite having the coarse energy resolution, this setup enables the assessment of the energy dependency of the emitted X-rays. This allows us to go from a situation where the signal is strongly line radiation

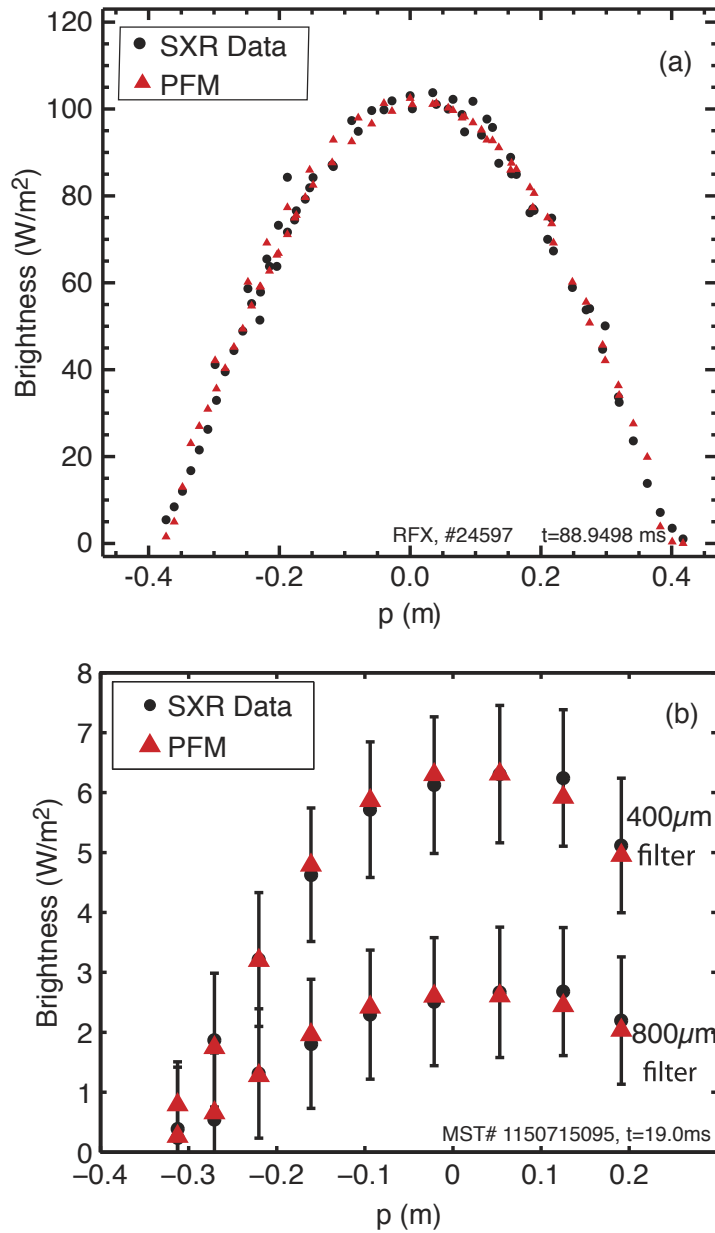


Fig. 2. An illustration of typical agreement between PFM (triangles, red) and SXR measurements (circles, black) plotted versus impact parameter in (a) RFX-mod and (b) MST after filtering out known line emission from Al.

dominated to a situation where the signal contains only free-free and radiative recombination. As can be seen in Fig. 4, different filters transmit different amounts of radiation from different sources.

Figure 4 shows the expected brightness for a chord going through the core of MST for four of the eight filters used in the experiment as a function of core T_e . For these plots, profiles based on typical experimental values were fixed for the underlying plasma parameters, and the on-axis

value of T_e was varied between 500 and 3200 eV. Each curve in the four plots shows the brightness for different sources of radiation. The thinnest filter used was 85 μm (Fig. 4a) and is clearly dominated by line radiation, and as the filter thickness gets thicker, the contributions from line and dielectronic recombination radiation get smaller until they are negligible for a 427- μm filter (Fig. 4d). In the experiment, the thickest filter used was 833 μm , but all filters thicker than 427 μm contain only free-free and

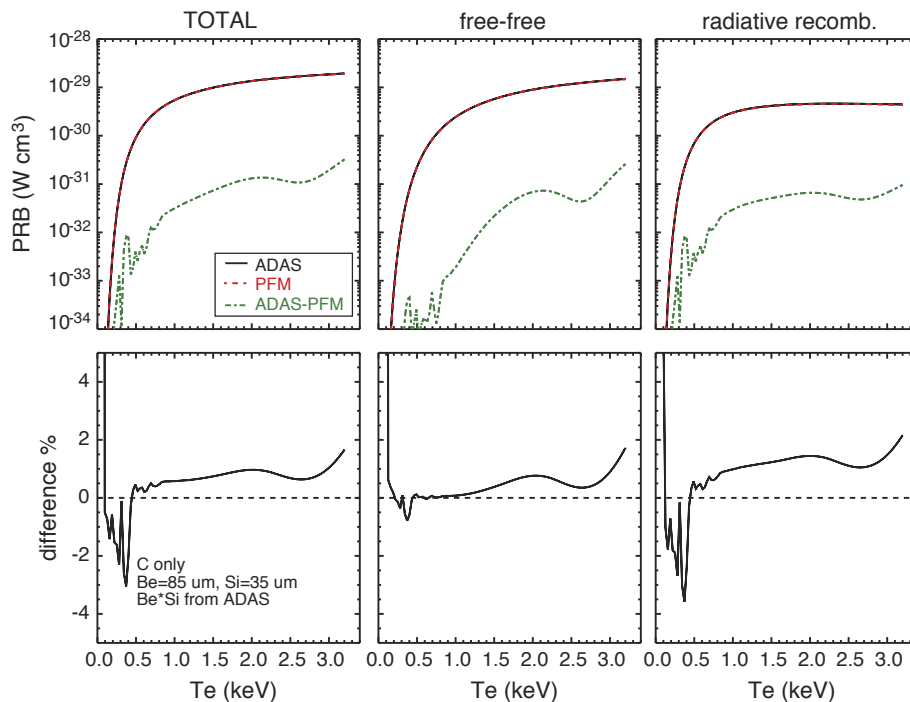


Fig. 3. Comparison of PRB between ADAS and PFM versus electron temperature. The top row shows the coefficient for ADAS (solid, black), PFM (dashed, red), and the difference between the two curves, (dot-dashed, green). The bottom row shows the percent difference relative to ADAS. Over a large range of temperatures, the two models agree to within 1% to 2%. Discrepancies for T_e below 500 eV are expected because assumptions in PFM are known to be violated.

radiative recombination radiation. It should be noted that the decrease in line radiation is smooth because the transmission curve for the Be filters is smooth.

Figure 4 gives some understanding of the relative amounts of radiation that we expect to measure for the eight filters for typical plasma parameters, but for an actual comparison to experiment, experimental data from the same shot should be used. Electron density and temperature profiles were measured using interferometry and Thomson scattering, respectively, and the neutral density profile was inferred from H- α measurements using a two-dimensional reconstruction technique³⁵ based on the DEGAS 2 Monte Carlo model.³⁶ The estimated uncertainty is 10% to 15% in the core. Impurity density profiles were not available but as previously mentioned have been well studied and are fairly similar for similar plasma conditions.^{18–20,29} As such, the profiles followed those found in Ref. 29.

The neutral density in MST can be quite high, leading to significant charge exchange between impurity ions and neutral hydrogen, so two comparisons were done. Figures 5 and 6 show the comparison between ADAS modeling and the experiment as a function of filter cutoff energy for diodes that view the plasma core. Figures 5 and 6 both show separated components of radiation as in

Fig. 4 in order to gain a sense of which sources of radiation are important in the experiment. Figure 5 shows the results when ignoring charge-exchange losses, and Fig. 6 shows the results when including charge-exchange losses.

Figures 5 clearly shows that ignoring charge-exchange losses in the plasma results in a brightness that is much too high at large cutoff energy (thick filters) and too low at low cutoff energy (thin filters). This is likely because the process of charge exchange with a neutral hydrogen affects the ionization balance of the ions, Al in particular. Since charge exchange tends to suppress the higher charge states, ignoring it leads to an overprediction of the number of fully ionized Al particles in the plasma. Fully ionized ions do not emit line radiation but rather emit more continuum radiation. The consequence is an overprediction of brightness at high cutoff energy where continuum radiation dominates and an underprediction at low cutoff energy where line radiation dominates.

This interpretation is further supported by the improved agreement present in Fig. 6, which includes the effect of charge-exchange losses due to neutral hydrogen in the plasma. ADAS calculates the effect of these neutral particles on the charge state fraction of Al, assuming all

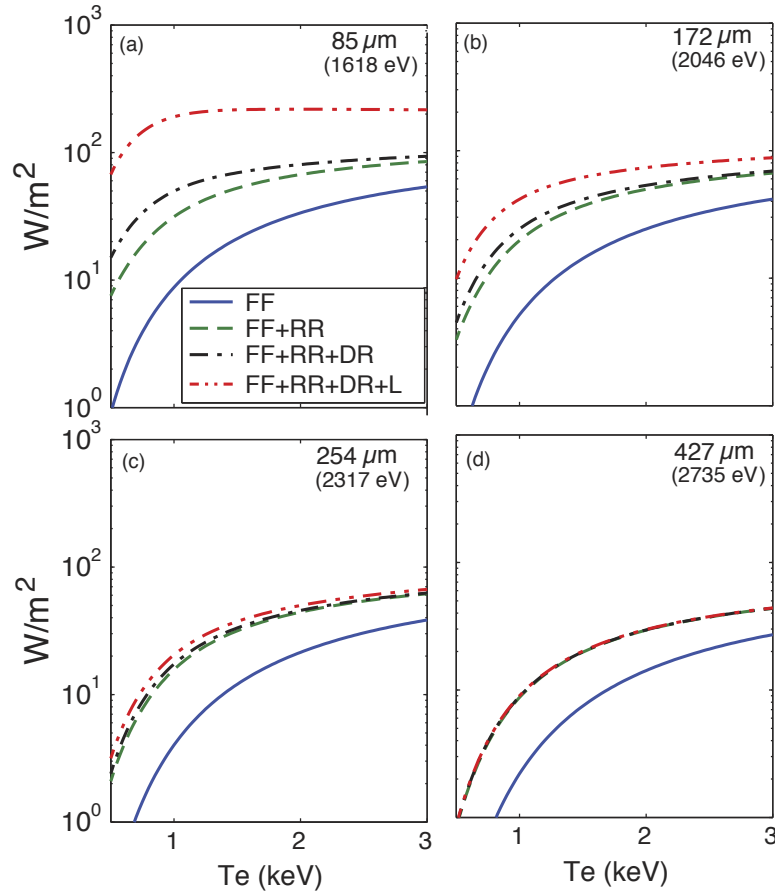


Fig. 4. The expected brightness for a chord going through the core of MST as a function of T_e for four of the eight filters used in experiment: (a) $85 \mu m$, (b) $172 \mu m$, (c) $254 \mu m$, and (d) $427 \mu m$. The 10% cut energy is listed in parentheses below the filter thickness. The solid curve (blue) shows the contribution from free-free radiation only, the dashed curve (green) shows free-free plus radiative recombination, the dash-dot (black) curve has free-free, radiative, and dielectronic recombination, and the dash-dot-dot (red) includes all previous sources plus line radiation. Profiles for the underlying plasma parameters were fixed based on typical experimental values, and the on-axis value of T_e was varied from 500 to 3200 eV.

neutral particles are in the ground state. The agreement in this case is quite good. A linear plot shown in Fig. 7 further illustrates the scale of agreement for the larger brightnesses, which are compressed on the log scale. Figures 6 and 7 also show that all sources of radiation must be included to match data from all filters simultaneously. It should be stressed that there were essentially no free parameters used. The impurity densities were varied within their known experimental uncertainties to account for possible shot-to-shot variance, but the other parameters were fixed from the experiment. Furthermore, impurity densities serve mainly to match the absolute magnitude of the signal but do not affect the energy dependence. Electron temperature, electron density, and neutral density most strongly affect the energy dependence, and these were all measured. This agreement between ADAS and the experiment for all

eight filters simultaneously is a strong indication that ADAS can accurately predict SXR brightness. And, while this is a preliminary comparison, these results indicate that ADAS is a suitable model for interpreting SXR brightness models.

IV. CONCLUSION

We have shown a cross verification of ADAS continuum radiation compared to the PFM in-house model. PFM has been used extensively as an aid in interpreting SXR brightness measurements, thus making it a good source for cross verification. ADAS and PFM agree with each other to within 1% to 2% for both free-free and radiative recombination. Combining these continuum measurements with resonant

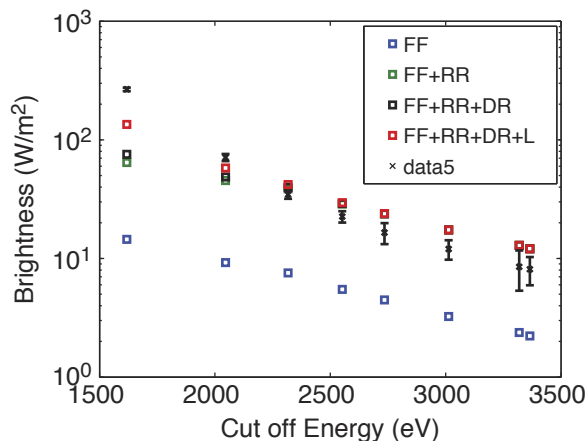


Fig. 5. Predicted brightness for eight filters (squares) versus filter cutoff energy compared to experimental SXR measurements (x) ignoring charge exchange with neutral particles. The coloring for the brightness predictions follows that in Fig. 4.

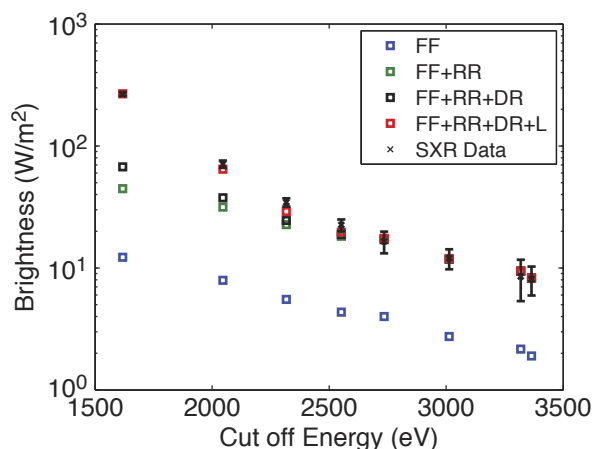


Fig. 6. Predicted brightness for eight filters (squares) versus filter cutoff energy compared to experimental SXR measurements (x) including charge exchange with neutral particles. The coloring for the brightness predictions follows that in Fig. 4.

sources of radiation (line radiation and dielectronic recombination radiation) to predict SXR brightness measurements indicates good agreement with experimental SXR measurements when charge-exchange effects are taken into account. The agreement seen spanned several different ranges in dominant physics, from signals that are line radiation dominated to signals that are continuum dominated. This comparison is a preliminary comparison of ADAS for SXR brightness measurements, though a more quantitative validation should be done. However, these preliminary results indicate that ADAS can be used effectively as an interpretive model for SXR brightness measurements and can aid in the

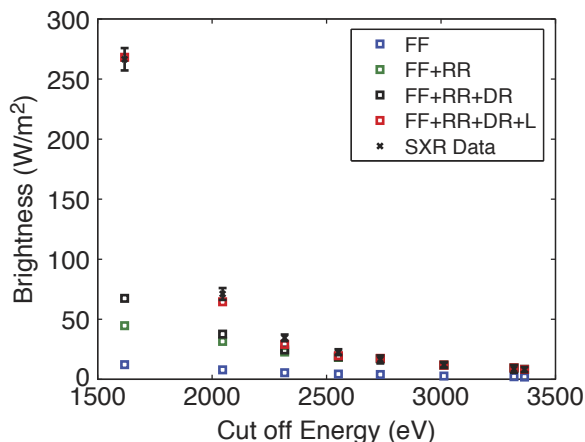


Fig. 7. Predicted brightness for eight filters (squares) versus filter cutoff energy compared to experimental SXR measurements (x) including charge exchange with neutral particles. The coloring for the brightness predictions follows that in Fig. 4.

extraction of quantitative information on n_z , n_e , T_e , and n_D . This analysis has immediate application to MST, but this work based on AI may be extendable to other medium- or high- Z impurities present in other machines.

Acknowledgment

This material is based upon work supported by the U.S. Department of Energy Office of Science, Office of Fusion Energy Sciences program under grants DE-FC02-05ER54814 and DE-SC0015474.

References

1. S. VON GOELER, W. STODIEK, and N. SAUTHOFF, "Studies of Internal Disruptions and $m = 1$ Oscillations in Tokamak Discharges with Soft-X-Ray Techniques," *Phys. Rev. Lett.*, **33**, 20, 1201 (1974); <https://doi.org/10.1103/PhysRevLett.33.1201>.
2. R. S. GRANETZ and J. F. CAMACHO, "X-Ray Tomography on Alcator C," *Nucl. Fusion*, **25**, 6, 727 (1985); <https://doi.org/10.1088/0029-5515/25/6/008>.
3. R. S. GRANETZ and P. SMEULDERS, "X-Ray Tomography on JET," *Nucl. Fusion*, **28**, 3, 457 (1988); <https://doi.org/10.1088/0029-5515/28/3/011>.
4. N. ASAKURA et al., "Soft X-Ray Measurements on the REPUTE-1 Reversed Field Pinch," *Nucl. Fusion*, **29**, 6, 893 (1989); <https://doi.org/10.1088/0029-5515/29/6/003>.
5. A. P. NAVARRO, M. A. OCHANDO, and A. WELLER, "Equilibrium-Based Iterative Tomography Technique for

- Soft X-Ray in Stellarators,” *IEEE Trans. Plasma Sci.*, **19**, 4, 569 (1991); <https://doi.org/10.1109/27.90321>.
6. F. C. JAHODA et al., “Continuum Radiation in the X Ray and Visible Regions from a Magnetically Compressed Plasma (Scylla),” *Phys. Rev.*, **119**, 3, 843 (1960); <https://doi.org/10.1103/PhysRev.119.843>.
 7. T. P. DONALDSON, “Theory of Foil-Absorption Techniques for Plasma X-Ray Continuum Measurements,” *Plasma Phys.*, **20**, 12, 1279 (1978); <https://doi.org/10.1088/0032-1028/20/12/005>.
 8. M. C. BORRÁS and R. S. GRANETZ, “Discrepancies Between Soft X-Ray Emissivity Contours and Magnetic Flux Surfaces in Alcator C-Mod,” *Plasma Phys. Control. Fusion*, **38**, 3, 289 (1996); <https://doi.org/10.1088/0741-3335/38/3/005>.
 9. R. GRANETZ and M. BORRÁS, “Is X-Ray Emissivity Constant on Magnetic Flux Surfaces?” *Fusion Eng. Des.*, **34–35**, 153 (1997); [https://doi.org/10.1016/S0920-3796\(96\)00682-5](https://doi.org/10.1016/S0920-3796(96)00682-5).
 10. H. CHEN et al., “Poloidally Asymmetric Distribution of Impurities in Joint European Torus Plasmas,” *Phys. Plasmas*, **7**, 11, 4567 (2000); <https://doi.org/10.1063/1.1311806>.
 11. H.-J. KUNZE, *Introduction to Plasma Spectroscopy*, Springer-Verlag, Berlin, Heidelberg (2009).
 12. H. P. SUMMERS et al., “Atomic Data for Modelling Fusion and Astrophysical Plasmas,” *Plasma Phys. Control. Fusion*, **44**, 12B, B323 (2002); <https://doi.org/10.1088/0741-3335/44/12B/323>.
 13. N. R. BADNELL et al., “Dielectronic Recombination Data for Dynamic Finite-Density Plasmas—I. Goals and Methodology,” *Astron. Astrophys.*, **406**, 3, 1151 (2003); <https://doi.org/10.1051/0004-6361:20030816>.
 14. H. P. SUMMERS et al., “Modelling Spectral Emission from Fusion Plasmas,” *AIP Conf. Proc.*, **1438**, 1, 181 (2012); <https://doi.org/10.1063/1.4707875>.
 15. A. GIUNTA et al., “Diagnosing Transient Plasma Status: From Solar Atmosphere to Tokamak Divertor,” *J. Instrum.*, **11**, 9, C09008 (2016); <https://doi.org/10.1088/1748-0221/11/09/C09008>.
 16. R. DEXTER et al., “The Madison Symmetric Torus,” *Fusion Technol.*, **19**, 131 (1991); <https://doi.org/10.13182/FST91-A29322>.
 17. B. CHAPMAN et al., “High Confinement Plasmas in the Madison Symmetric Torus Reversed-Field Pinch,” *Phys. Plasmas*, **9**, 2061 (2002); <https://doi.org/10.1063/1.1456930>.
 18. S. T. A. KUMAR et al., “Classical Confinement and Outward Convection of Impurity Ions in the MST RFP,” *Phys. Plasmas*, **19**, 5, 056121 (2012); <https://doi.org/10.1063/1.4718310>.
 19. S. T. A. KUMAR et al., “High Resolution Charge-Exchange Spectroscopic Measurements of Aluminum Impurity Ions in a High Temperature Plasma,” *Plasma Phys. Control. Fusion*, **54**, 1, 012002 (2012); <https://doi.org/10.1088/0741-3335/54/1/012002>.
 20. T. BARBUI et al., “Impurity Transport Studies in the Madison Symmetric Torus Reversed-Field Pinch During Standard and Pulsed Poloidal Current Drive Regimes,” *Plasma Phys. Control. Fusion*, **56**, 7, 075012 (2014); <https://doi.org/10.1088/0741-3335/56/7/075012>.
 21. H. P. SUMMERS, “The ADAS User Manual” (2004); <http://www.adas.ac.uk/manual.php>.
 22. M. G. VON HELLERMANN et al., “Complex Spectra in Fusion Plasmas,” *Phys. Scr.*, **2005**, T120, 19 (2005); <https://doi.org/10.1088/0031-8949/2005/T120/003>.
 23. H. P. SUMMERS et al., “Ionization State, Excited Populations and Emission of Impurities in Dynamic Finite Density Plasmas: I. The Generalized Collisional-Radiative Model for Light Elements,” *Plasma Phys. Control. Fusion*, **48**, 2, 263 (2006); <https://doi.org/10.1088/0741-3335/48/2/007>.
 24. S. D. LOCH et al., “The Effects of Radiative Cascades on the X-Ray Diagnostic Lines of Fe 16+,” *J. Phys. B*, **39**, 1, 85 (2006); <https://doi.org/10.1088/0953-4075/39/1/009>.
 25. A. S. GIUNTA et al., “Comparison Between Observed and Theoretical OIV Line Ratios in the UV/EUV Solar Spectrum as Derived by SUMER, CDS and EIS,” *Astron. Astrophys.*, **538**, A88 (2012); <https://doi.org/10.1051/0004-6361/201118178>.
 26. S. S. HENDERSON et al., “Optimisation and Assessment of Theoretical Impurity Line Power Coefficients Relevant to ITER and DEMO,” *Plasma Phys. Control. Fusion*, **59**, 5, 055010 (2017); <https://doi.org/10.1088/1361-6587/aa6273>.
 27. H. P. SUMMERS and R. W. P. McWHIRTER, “Radiative Power Loss from Laboratory and Astrophysical Plasmas. I. Power Loss from Plasmas in Steady-State Ionisation Balance,” *J. Phys. B*, **12**, 14, 2387 (1979); <https://doi.org/10.1088/0022-3700/12/14/022>.
 28. F. BONOMO et al., “2D Characterization of Core Thermal Topology Changes in Controlled RFX-mod QSH States,” *Nucl. Fusion*, **49**, 4, 045011 (2009); <https://doi.org/10.1088/0029-5515/49/4/045011>.
 29. M. GALANTE et al., “Determination of Z_{eff} by Integrating Measurements from X-Ray Tomography and Charge Exchange Recombination Spectroscopy,” *Nucl. Fusion*, **55**, 12, 123016 (2015); <https://doi.org/10.1088/0029-5515/55/12/123016>.
 30. I. H. HUTCHINSON, *Principles of Plasma Diagnostics*, 2nd ed., “Electromagnetic Emission by Free Electrons,” Chap. 6, p. 155, Cambridge University Press (2002).
 31. P. A. M. VAN HOOFF et al., “Accurate Determination of the Free-Free Gaunt Factor—I. Non-Relativistic Gaunt Factors,” *Monthly Notices R. Astron. Soc.*, **444**, 1, 420 (2014); <https://doi.org/10.1093/mnras/stu1438>.

32. W. J. KARZAS and R. LATTER, “Electron Radiative Transitions in a Coulomb Field,” *Astrophys. J. Supp. Ser.*, **6**, 167 (1961); <https://doi.org/10.1086/190063>.
33. M. B. MCGARRY et al., “A New Double-Foil Soft X-Ray Array to Measure T_e on the MST Reversed Field Pinch,” *Rev. Sci. Instrum.*, **81**, 10, 10E516 (2010); <https://doi.org/10.1063/1.3481167>.
34. M. B. MCGARRY et al., “High-Performance Double-Filter Soft X-Ray Diagnostic for Measurement of Electron Temperature Structure and Dynamics,” *Rev. Sci. Instrum.*, **83**, 10, 10E129 (2012); <https://doi.org/10.1063/1.4740274>.
35. Z. XING et al., “Neutral Dynamics and Ion Energy Transport in MST Plasma,” *Proc. 57th Annu. Mtg. APS Division of Plasma Physics*, Savannah, Georgia, November 16–20, 2015, American Physical Society (2015).
36. D. STOTLER et al., “The DEGAS 2 Users Manual,” Princeton Plasma Physics Laboratory (2013).